Journal of Power Sources 369 (2017) 95–102

Contents lists available at ScienceDirect

Journal of Power Sources

journal homepage: www.elsevier.com/locate/jpowsour

$Na_{2.5}Fe_{1.75}(SO_4)_3$/Ketjen/rGO: An advanced cathode composite for sodium ion batteries

A. Goñi [a, b], A. Iturrondobeitia [a], I. Gil de Muro [a, b], L. Lezama [a, b], T. Rojo [a, c, *]

[a] Departamento de Química Inorgánica, Universidad del País Vasco UPV/EHU, P.O. Box 644, 48080, Bilbao, Spain
[b] BCMATERIALS, Ibaizabal Bidea 500, Parque Científico y Tecnológico de Bizkaia, 48160, Derio, Spain
[c] CIC energiGUNE, Parque Tecnolóogico de Álava, Albert Einstein 48, 01510, Miñano, Álava, Spain

HIGHLIGHTS

- Advanced cathode composite.
- $Na_{2.5}Fe_{1.75}(SO_4)_3$/Ketjen/rGO.
- Good rate capability.
- Great cycling stability.
- SEI layer.

ARTICLE INFO

Article history:
Received 13 July 2017
Received in revised form
15 September 2017
Accepted 30 September 2017
Available online 9 October 2017

Keywords:
Graphene
Composite
Advanced cathode
Iron sulfate
High voltage
Post mortem study

ABSTRACT

An advanced cathode composite $Na_{2.5}Fe_{1.75}(SO_4)_3$/Ketjen/rGO for sodium ion batteries has been prepared, joining together the excellent electrochemical properties of the three components: off stoichiometric iron sulfate alluaudite, Ketjen Black carbon and reduced graphene oxide (rGO).

This electrode material has been exhaustively characterized by XRD, thermogravimetric analysis, Raman spectroscopy and SEM and TEM microscopy. The study has demonstrated that a high quality electrode material has been designed containing a porous sulfate core properly coated by interweaved rGO fibers and Ketjen Black nanoparticles. The electrochemical study has revealed an excellent performance providing specific capacities close to the theoretical one at 1C. Additionally, this composite has shown a very good rate capability and a great cycling stability for at least 200 cycles maintaining a coulombic efficiency of 96%.

The post mortem analysis, which includes EPR and XPS measurements, has demonstrated that the carbonaceous coating on the composite generates a stable and protective SEI layer over the active material guaranteeing a successful performance during a long cycle life.

1. Introduction

At the present time the reliable practical application of sodium ion batteries (SIBs) needs the optimization of all the components, accounting for electrolyte and electrode materials [1]. Safe and accessible cathode compounds with high operating voltage, large specific capacity, and good cycling stability will be a key factor in order to surpass the good performance of the lithium ion batteries (LIBs) [2,3].

Various cathode materials have been reported up to now [4]. Among them, layer and tunnel type transition metal oxides, transition metal sulfides and fluorides, Prussian blue analogues, polymers, and polyanionic compounds, such as phosphates, pyrophosphates and sulfates, have received increased attention during the last years [5]. In this context, Fe-based alluaudite phases have demonstrated to be suitable candidates for the reversible redox extraction-insertion of sodium ions providing a good electrochemical performance [6]. Barpanda et al. [7] published the first alluaudite-type sulfate, $Na_2Fe_2(SO_4)_3$, registering a high Fe^{3+}/Fe^{2+} redox potential at 3.8 V along with fast rate kinetics. Moreover, that phase possesses an inherent deviation from stoichiometry leading to $Na_{2+2x}Fe_{2-x}(SO_4)_3$ compound, which has emerged as a more

* Corresponding author. Departamento de Química Inorgánica, Universidad del País Vasco UPV/EHU, P.O. Box 644, 48080, Bilbao, Spain.
E-mail address: trojo@cicenergigune.com (T. Rojo).

https://doi.org/10.1016/j.jpowsour.2017.09.087
0378-7753/

promising cathode material due to its enhanced compositional, structural and electrochemical flexibility [8].

As typical for alluaudite compounds, $Na_{2+2x}Fe_{2-x}(SO_4)_3$ adopts a monoclinic lattice with $C2/c$ symmetry. In this structure, edge shared FeO_6 octahedra are linked with SO_4 units in a corner-sharing fashion, which generates a three-dimensional network with large tunnels along the c-axis with sodiums located in the tunnels [9]. During the charge and discharge processes, the structure undergoes through a reversible single phase reaction where the sodiums are extracted sequentially from different positions in the structure (Na1, Na2 and Na3) [10,11]. In the first charge, primarily, Na3 sites are evacuated followed by the Na1 and then the Na2 sites. Afterwards, in the first discharge, the sodium insertion occurs successively at Na2, Na3 and Na1 sites. This dynamics is reversible in subsequent cycles [12]. Moreover, an initial structural rearrangement takes place upon the first charge, where a small amount of Fe irreversibly migrates from its original site to Na1 position. Based on one-electron transfer, this material is able to deliver approximately 85% of its theoretical capacity (106 $mAh.g^{-1}$) and has a moderate rate capability.

Regarding the preparation of this sulfate, $Na_{2+2x}Fe_{2-x}(SO_4)_3$ can be easily synthesized and scaled up by using low temperature solid-state methods, although care should be taken on its hygroscopic nature [13]. In order to optimize the electrochemical properties of this cathode compound, some efforts have been made to prepare composites by mixing selected constituents. A study has been reported on sodium iron sulfate nanoparticles anchored to single-wall carbon nanotubes (SWNT). These SWNTs constitute a 3D based framework that enhances the electron/ion transport properties and improves the sodium intercalation kinetics [14]. Moreover, the same research group has reported a large-scalable approach to construct a freestanding alluaudite $Na_{2+2x}Fe_{2-x}(SO_4)_3$@porous carbon nanofiber (PCNF) hybrid film. Here, the highly porous graphitic-like carbon-nanofibers wrap the sulfate particles giving place to a hybrid network. The material has demonstrated to have a long cycle life and rate capability [15].

Considering the promising graphene-based technologies which are being developed for energy applications, the employment of graphene as a component of the cathode composite may represent an important improvement. This material has a flexible planar carbon atom structure, a strong chemical durability, an outstanding specific surface area and a high electrical conductivity [16], and it has a low cost when compared to other related materials as could be the SWNTs. Moreover, it has already been demonstrated that this material has a good electrochemical behavior when using it as anode material for SIBs [17]. Thus, all these factors make it an attractive candidate as a constituent of electrode composites. On the other hand, Ketjen Black carbon is another effective component that is usually added to electrode mixtures, as it enhances both, the connection between the active material particles and the electronic conductivity. In this sense, the strategy of mixing graphene and Ketjen Black with the alluaudite $Na_{2.5}Fe_{1.75}(SO_4)_3$ sulfate phase should induce the emergence of the best qualities of this active material. In addition, due to their hydrophobic nature, these carbonaceous components could act as protectors against humidity, increasing therefore the stability of the electrode material in atmospheric conditions.

In this article we report on the synthesis and exhaustive characterization of an advanced cathode composite for SIBs: $Na_{2.5}Fe_{1.75}(SO_4)_3$/Ketjen/rGO. The morphology, spectroscopic and electrochemical properties have been studied obtaining excellent results. Moreover, a post mortem study of the cycled electrodes has been performed by EPR and XPS techniques in order to further analyze the SEI formation so as to design a next generation SIB.

2. Experimental

2.1. Sample preparation

For the preparation of $Na_{2.5}Fe_{1.75}(SO_4)_3$/Ketjen/rGO composite a procedure involving different steps was followed. First of all, all the carbonaceous components were mixed: 0.05 g of Ketjen Black (Akzonobel) were added to 8 ml of a GO water dispersion (4 mg/ml concentration) (graphene oxide, Graphenea). Additionally, 0.176 g of ascorbic acid (Sigma-Aldrich) were also dissolved in order to induce the reduction of GO. The resulting suspension was sonicated at 75° C for one hour. Afterwards, a black spongy monolith was obtained inside a clear water solution. That monolith was recovered from solution and dried at 25 °C. The resulting carbon powder was mixed in an agate mortar with 0.9731 g of $FeSO_4.7H_2O$ (Sigma-Aldrich), 0.3551 g of Na_2SO_4 (Lab-Kem) and acetone. The as-obtained dough was subjected to a single heat treatment at 350 °C for 8 h under nitrogen atmosphere.

$Na_{2.5}Fe_{1.75}(SO_4)_3$/Ketjen and $Na_{2.5}Fe_{1.75}(SO_4)_3$/rGO control samples were prepared following the same synthesis method that was used for $Na_{2.5}Fe_{1.75}(SO_4)_3$/Ketjen/rGO composite. Nevertheless, in these cases one of the carbonaceous components (rGO or Ketjen) was omitted.

2.2. Characterization

A Perkin-Elmer 2400CHN analyzer was employed to determine the carbon content of the sample. The structural characterization was carried out by X-ray powder diffraction with a Bruker D8 Advance Vario diffractometer using CuKα radiation. The obtained diffractograms were profile-fitted using the FullProf program [18]. Thermogravimetric analysis was performed with a Netzsch STA 449 C equipment, in Ar atmosphere with a heating rate of 5 °C/min. Raman measurements were carried out with a Confocal Raman Microscope made by Renishaw. The morphologies of the materials were studied by Transmission Electron Microscopy (TEM) using a Philips CM200 microscope and by Scanning Electron Microscopy (SEM) (Carl Zeiss EVO-40 equipment).

2032 coin cells were assembled to evaluate the electrochemical performance. To prepare the electrode, the active material was mixed with conducting Akzonobel Ketjen Black and polyvinylidene fluoride (PVDF) binder with weight ratios of 80:10:10 and dispersed in *N*-methyl-2-pyrrolidone (NMP) to form a slurry. The slurry was then cast onto Al current collector and dried at 120 °C in a vacuum oven overnight. Electrochemical cells with metallic sodium foils as counter electrodes, Whatman GF/A glass microfiber separators, and 1 M $NaPF_6$ in 50%–50% ethyl carbonate (EC) and dimethyl carbonate (DMC) solution with 1 wt % FEC as the electrolyte solution were assembled in an Ar-filled glove box. The electrochemical measurements were carried out on a Bio-Logic VMP3 potentiostat/galvanostat battery tester at room temperature. Typical electrode loadings were 1.0 mg/cm^2. The galvanostatic charge/discharge experiments were performed between 2.0 and 4.5 V at 0.1C, 1C, 2C and 5C current rates. To calculate the capacity values, only the alluaudite phase was considered as active material, not including the carbon from the composite.

For the post-mortem analysis of the cycled electrodes, cells were disassembled in an Ar-filled glove box. The positive electrode tapes were washed during a few seconds three times with a large excess of dimethyl carbonate (DMC) in order to remove impurities. The harvested electrodes were used for further analysis, such as EPR and XPS measurements. EPR spectra were recorded at X-band frequency with a Bruker ESP300 spectrometer. X-ray Photoelectron Spectroscopy (XPS) was performed using a SPECS equipment comprising an energy-analyzer Phoibos 1D-DLD 150.

3. Results and discussion

The whole amount of carbon in the $Na_{2.5}Fe_{1.75}(SO_4)_3$/Ketjen/rGO composite was determined by elemental analysis, obtaining a value of 9.45%. Taking into account that graphene was added in the required quantity in order to match a 3.5% of the composite weight, it could be said that the remaining ~6% should correspond to the amorphous carbon.

Fig. 1a) shows the experimental and profile-fitted XRD patterns of the composite. Most of the diffraction peaks could be indexed to the monoclinic alluaudite *C*2/*c* space group. The values of the cell parameters obtained from profile-fitting the pattern with Fullprof-Suite program (see reference [18]) are a = 12.672(2) Å, b = 12.781(2) Å, c = 6.524(1) Å and β = 115.65(1)°, being in good agreement with the crystal structure of an off-stoichiometric alluaudite-type sodium iron sulfate.

An additional reflection can be detected at 2θ ≈ 25.9° which could be attributed to the characteristic (002) peak of the reduced graphene oxide (rGO). This fact together with the absence of a diffraction peak at 2θ ≈ 11° suggest that the GO has been reduced to rGO due to the action of the ascorbic acid [19].

One of the main handicaps for employing iron sulfates as electrode materials is probably their hygroscopic character. This way, in order to verify if carbon components (Ketjen Black and rGO) offer some type of protection against the ambient humidity, XRD patterns of $Na_{2.5}Fe_{1.75}(SO_4)_3$/Ketjen/rGO sample were registered every three hours during a day at atmospheric conditions (Fig. 1b). No changes in diffraction maxima intensity or position neither additional reflection were observed along the time. Consequently, it could be concluded that this material is stable enough to be manipulated without any special requirements. This advantage could be attributed to the hydrophobic carbonaceous constituents in the composite, which probably act as protectors against humidity.

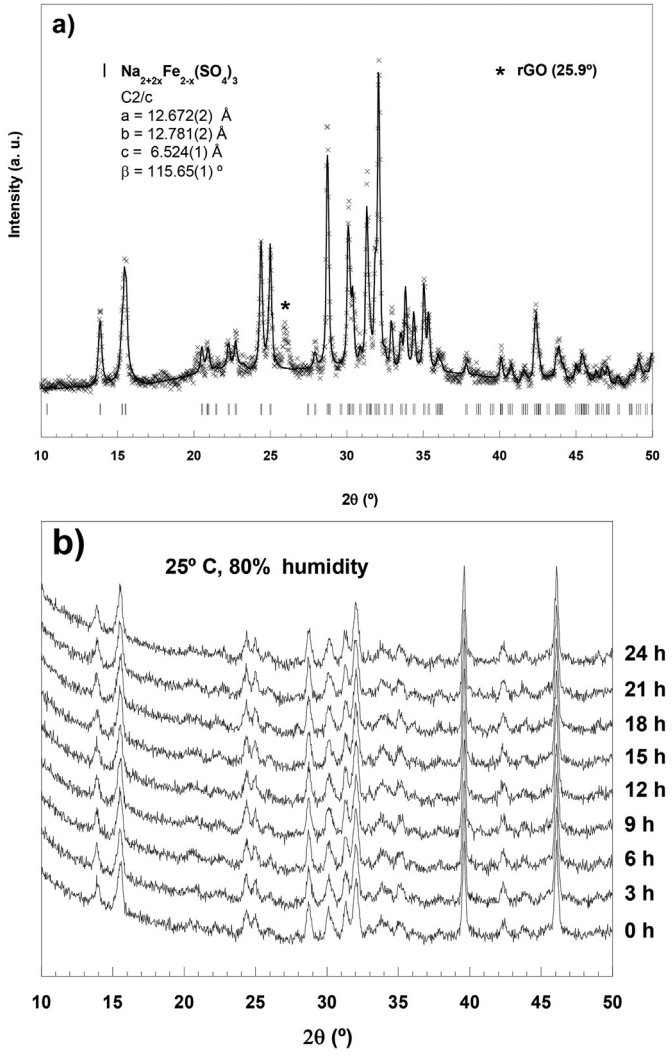

Fig. 1. a) XRD pattern of $Na_{2.5}Fe_{1.75}(SO_4)_3$/Ketjen/rGO sample. b) XRD patterns of $Na_{2.5}Fe_{1.75}(SO_4)_3$/Ketjen/rGO, registered every three hours during a day at atmospheric conditions.

Thermogravimetric analysis (TGA) was used to test the thermal stability of the composite as well as to corroborate the reduction of GO to rGO. No noticeable mass loss can be detected until 450° C. At this point the onset of decomposition starts for the $Na_{2.5}Fe_{1.75}(SO_4)_3$ compound, releasing SO_x gases, being in good agreement with the results observed in the literature [20].

GO containing samples usually show a significant weight loss around 100 or 200 °C due to the release of CO, CO_2 and steam, which come from the decomposition of the most labile functional groups. In contrast, the samples containing rGO show a higher thermal stability due to the absence of most of the functional groups that contain oxygen [21]. In the present case, even though the composite was synthesized at 350° C, it was found to be stable up to 450° C. At this point, the sulfate group starts to disintegrate. Nevertheless, it is remarkable that no previous mass loss ascribable to the releasing of functional groups coming from GO is observed.

Fig. 2 shows the Raman spectrum of the composite. The prominent peaks located at ~1350 cm^{-1} and ~1585 cm^{-1} can be attributed to the D and G bands, which are characteristic of carbonaceous compounds. The intense and fairly narrow G band arises due to the in-plane bond-stretching motion of sp^2 hybridized C atoms from both rGO and Ketjen Black. The broad D band, attributed to defects in carbon layers, such as the disruption in the sp^2 bonding, wrinkle formation or the presence of functional groups, comprises the superimposed signals corresponding to both of the different carbonaceous species in the composite.

The D′ band, also associated with defects, is observed close to 1620 cm^{-1} merged with the G band. The wide band extending from 2500 cm^{-1}–3200 cm^{-1} contains three peaks located at 2670 cm^{-1}, 2930 cm^{-1} and 3170 cm^{-1}, respectively. The peak at ~2670 cm^{-1} is known as the 2D (or G′) band since it is an overtone of the D band. Unlike the intense and lorentzian shaped 2D peak of a perfect

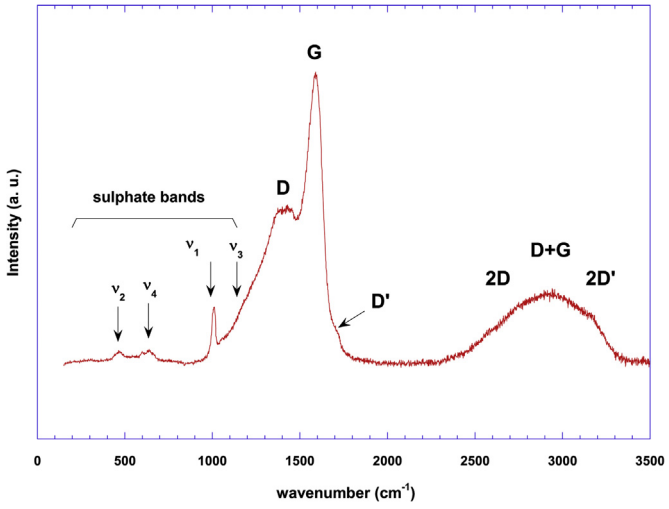

Fig. 2. Raman spectrum of $Na_{2.5}Fe_{1.75}(SO_4)_3$/Ketjen/rGO sample.

monolayer graphene, the 2D peak of few layered graphene is less intense and more complex in shape. In this sense, the presence of an intense D band and a weak 2D band is a general characteristic of graphenes produced by synthesis methods that involve an oxidation process followed by a reduction as it is in the present case. The peak around 2930 cm^{-1} is a combination mode of G and D bands, often referred as the D + G band. The hump situated around 3170 cm^{-1} is attributed to an overtone of the D′ band (2D′).

The raman spectrum of this sample is in good agreement with the presence of the disordered graphitic like Ketjen Black carbon and with the existence of a few layered rGO. Moreover, the active vibration modes of the sulfate group can also be observed [22]. This way, the stretching $\nu_1(SO_4)$ band is present at 1010 cm^{-1} and the bending modes $\nu_2(SO_4)$ and $\nu_4(SO_4)$ are located at 467 and 630 cm^{-1}, respectively. It is important to mention that the signal corresponding to the stretching of the compound, $\nu_3(SO_4)$, is overlapped with the D band from carbon.

The morphology of the composite was analyzed by SEM and TEM. As shown in Fig. 3a, the low-resolution SEM image displays an apparent compact and homogeneous material in which the different components, rGO, Ketjen Black and the sulfate phase, cannot easily distinguish. However, TEM micrographs (Fig. 3b, c and d) allow perceiving the real open nature of the composite, where all the components can be identified.

As can be observed in Fig. 3b, the sulfate particles seem to be sintered into a highly porous frame in which the pore sizes ranges from 10 to 20 nm. Additionally, the Ketjen Black particles and the reduced graphene oxide sheets can be clearly noticed in that framework on the edges of the bulk material (Fig. 3c). This way, the three constituent compounds are intimately connected between each other. Fig. 3d shows a detailed micrograph corresponding to the structure of the few layered rGO. The observed Ketjen black particle that is linked to graphene presents the characteristic turbostratic stacking structure.

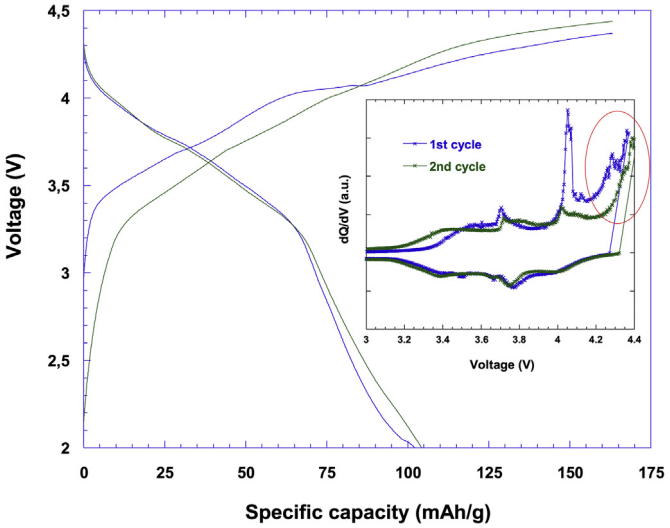

Fig. 4. First and second charge-discharge curves for $Na_{2.5}Fe_{1.75}(SO_4)_3$/Ketjen/rGO composite at C/10. The corresponding differential galvanostatic profiles (dQ/dV) are shown in the inset.

To evaluate the electrochemical performance of the composite, sodium half cells were charging and discharging, initially at C/10 current rate, in the voltage range 2.0–4.5 V. The first two charge/discharge curves and the corresponding differential galvanostatic

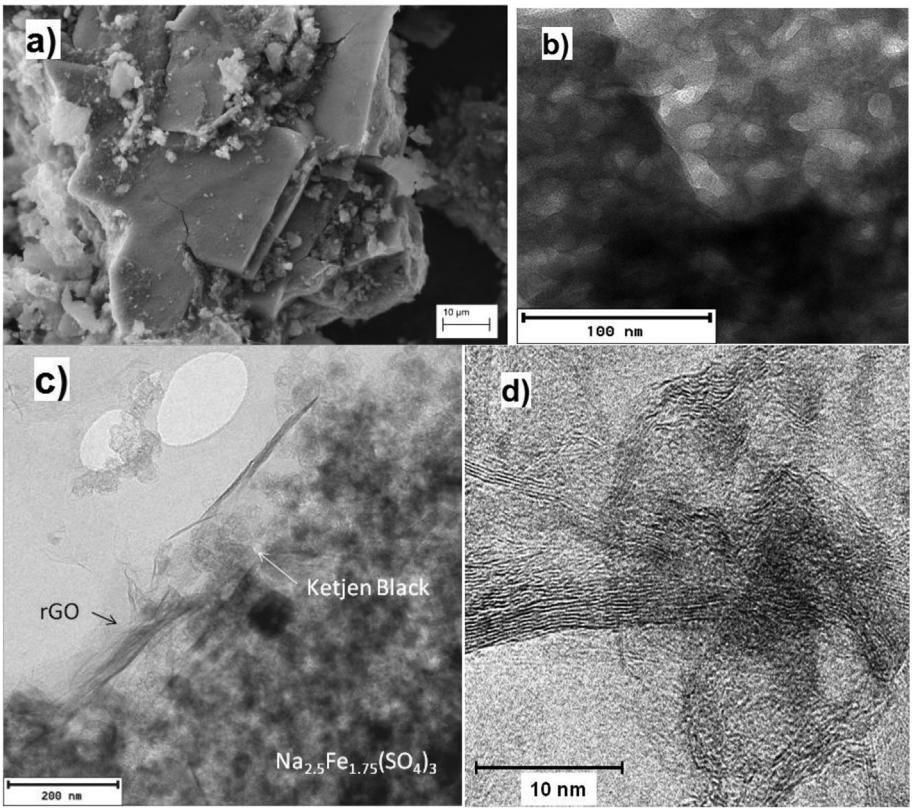

Fig. 3. a) SEM image of $Na_{2.5}Fe_{1.75}(SO_4)_3$/Ketjen/rGO, b) TEM micrograph of the sintered sulfate particles into a highly porous frame, c) TEM image displaying the distribution of the three components constituting $Na_{2.5}Fe_{1.75}(SO_4)_3$/Ketjen/rGO composite, and d) detailed TEM micrograph of the few layered rGO linked to a Ketjen black particle.

profiles (dQ/dV) of the composite are shown in Fig. 4. As it can be observed, at this discharge rate the material provides a specific capacity ~104 mAh/g, which is similar to the theoretical one (106 mAh/g).

On the first charge, the dQ/dV curve (blue line in the inset of Fig. 7) shows two main oxidation peaks at 3.70 and 4.06 V, together with some other slight anomalies, and a rough and deep final rise which has not been observed for alluaudites up to now. Therefore, that latter phenomenon could be attributed to the presence of graphene.

As previously mentioned in the introduction, the first desodiation involves the migration of some Fe atoms from the Fe1 site to the Na1 site. In this regard, this process has been associated with the sharp oxidation peak located at 4.06 V. In the subsequent discharge process, the reduction peaks situated at 3.97, 3.80 and 3.38 V have been attributed to the Na insertion into Na2, Na3 and the vacant Fe1/Na1 sites, respectively. On the second charge, the electrochemical reaction concerning the $Na_{2.5}Fe_{1.75}(SO_4)_3$ active phase is reversible, tracing the preceding discharge step. Here, a sequential extraction of Na ions occurs in the order of Na/Fe1 sites followed by the Na3 and Na2 sites, being in good agreement with the three broad peaks present in the dQ/dV plot. It is important to note that the structural and the Fe^{3+}/Fe^{2+} redox reversibility are retained upon the subsequent cycles.

The additional oxidation process that has been observed for the $Na_{2.5}Fe_{1.75}(SO_4)_3$/Ketjen/rGO composite material at high voltages (marked in red in the inset of Fig. 4), implies an irreversible additional capacity in the charge process. In this context, it is important to note that graphene, like graphite, is a redox-amphoteric species and therefore, it can be electrochemically reduced and oxidized at specific potentials. This way, it has been reported that the oxidation of graphene takes place at high voltages over 4.1 V accepting or intercalating anionic species such as PF_6^- from the electrolyte [23]. This fact increases the charge capacity of the electrode material but remarkably decreases the coulombic efficiency, as the consumed capacity is not recovered on discharging. Although in the first cycle the oxidation of graphene starts at 4.15 V, in the second cycle that process is moved towards higher voltage values such as 4.3 V, at C/10 rate. It is interesting to note that when increasing the charge/discharge rates up to 1C, that extra and irreversible capacity obtained on the charge process is vanished probably due to be ousted from the established voltage window.

To further investigate the electrochemical response of the composite material, a charge and discharge study at different rates was carried out. Fig. 5a shows the profile of the curves at 1C, 2C and 5C rates. The rate performance was tested recording 10 cycles at each different discharge rate in the range from 1C to 5C and back down, as shown in Fig. 5b.

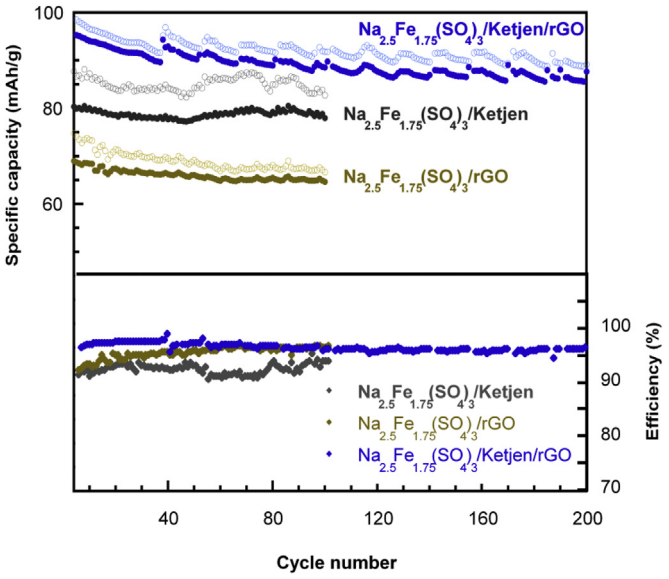

Fig. 6. Cycling performances of the $Na_{2.5}Fe_{1.75}(SO_4)_3$/Ketjen/rGO composite, and $Na_{2.5}Fe_{1.75}(SO_4)_3$/Ketjen and $Na_{2.5}Fe_{1.75}(SO_4)_3$/rGO as control samples at 1C.

As it could be expected, the cell shows a decreased capacity at the higher rate. Nevertheless, the sample delivers beyond 70 mAh/g when charging and discharging it at 5C. Moreover, when reducing the working rate back to 1C, the composite successfully recovers the capacity delivered in previous cycles. Taking into account the high average voltage at which the cell operates and the specific capacity that this one provides, the experimental value for the energy density is ~335 Wh/kg at 1C.

The cycling performance of the $Na_{2.5}Fe_{1.75}(SO_4)_3$/Ketjen/rGO cathode material was investigated at a current rate of 1C during 200 cycles. The values of the specific capacities on the successive charge/discharge cycles and the corresponding coulombic efficiency data have been represented in Fig. 6. As it can be noticed, the $Na_{2.5}Fe_{1.75}(SO_4)_3$/Ketjen/rGO sample retains a reversible specific capacity above 85 mAh/g for at least 200 cycles. Additionally, the

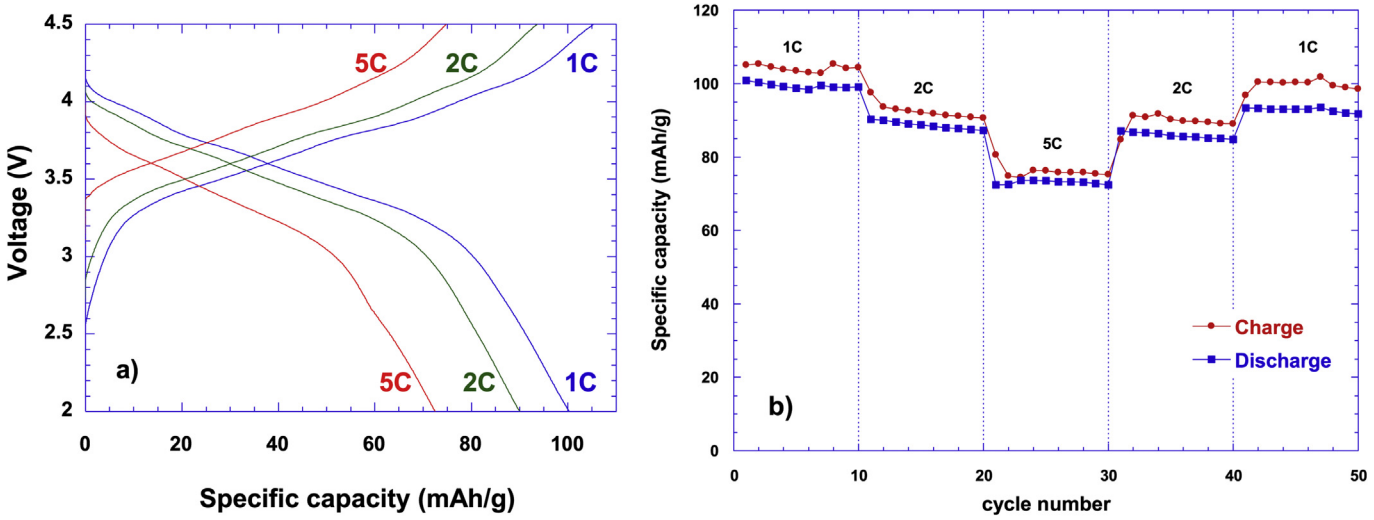

Fig. 5. Rate discharge capabilities for $Na_{2.5}Fe_{1.75}(SO_4)_3$/Ketjen/rGO material: a) profile of charge-discharge curves at 1C, 2C and 5C, b) specific capacity values at different rates.

coulombic efficiency also maintains a percentage value of 96%. It is important to note that the periodic discontinuity that can be appreciated every 12–14 cycles could probably be attributed to the temperature changes in the laboratory due to the heating of the room during the day.

In order to better understand the role and effects of Ketjen black and rGO, two control electrodes, both containing the active sulfate but only one of the carbonaceous components ($Na_{2.5}Fe_{1.75}(SO_4)_3$/Ketjen and $Na_{2.5}Fe_{1.75}(SO_4)_3$/rGO), were also studied for 100 cycles at 1C. The collected data for the charge and discharge cycles and coulombic efficiency can be observed in Fig. 6. Considering the specific capacity values reported for the bare $Na_{2.5}Fe_{1.75}(SO_4)_3$ compound (~50 mAh/g at 1C [see reference [13]], or ~ 80 mAh/g discharging at 1C but charging at C/10 [see reference [7]]), the addition of any of the carbonaceous species contributes to the improvement of the electrochemical performance. After 100 cycles at 1C, $Na_{2.5}Fe_{1.75}(SO_4)_3$/rGO still provides 67 mAh/g, while $Na_{2.5}Fe_{1.75}(SO_4)_3$/Ketjen delivers 79 mAh/g. Consequently, it can be said that the addition of Ketjen in the synthesis process clearly strengthens the capacity. On the other hand, the main effect caused by the addition of the rGO is observed in the coulombic efficiency as the value of this one is increased up to 98% after few cycles. This way, the addition of both of the carbonaceous sources has a synergistic effect favouring the electrochemical performance of the $Na_{2.5}Fe_{1.75}(SO_4)_3$/Ketjen/rGO sulfate phase.

3.1. Post mortem study

In order to better understanding the excellent electrochemical performance of the $Na_{2.5}Fe_{1.75}(SO_4)_3$/Ketjen/rGO cathode material, two half cells were disassembled to perform a post mortem study. One of the cells was stopped at the charged configuration at 4.5 V and the other at the discharged configuration at 2.0 V. This way, the recovered electrodes from the cells were washed with DMC and used for further characterization by EPR and XPS techniques.

The powder X-band EPR spectra of the charged and discharged electrode materials were measured at room temperature. The discharged sample only presents a nearly negligible signal at $g = 2.0$ which does not correspond to the main mass of the composite. At 2.0 V, the $Na_{2.5}Fe_{1.75}(SO_4)_3$ active material is in the reduced state and the ferrous species are not able to show any resonance signal. The Fe^{2+} non-Kramers ions exhibit short spin-lattice relaxation times and large zero-field splitting, which hinders the detection of any EPR data. Moreover, even if some Fe^{3+} proportion would be present in the compound, the detection by EPR would be difficult as the magnetic coupling between both iron species, Fe^{2+} and Fe^{3+}, in the same phase would impede the observation of any resonance band.

On the contrary, two different signals can be distinguish for the charged sample. The broadest one, with a g value of 2.00, and a peak-to-peak line width of $H \approx 140$ Gauss, is consistent with the presence of high spin Fe^{3+} in a slightly distorted octahedral symmetry. This fact corroborates the complete oxidation of the iron by the extraction of Na^+, since the influence of Fe^{2+} on EPR has been dissipated when the sample is charged. The other narrower contribution might correspond to free radical species, with a g value of 2.007 and a peak-to-peak line width of $H = 6$ Gauss. The radical species could arise from the oxidation process of graphene at high voltage in order to adopt the C^{n+} oxidized state. That narrow EPR signal is almost vanished for the discharged material, which probably could be attributed to the neutrality that graphene has recovered at 2 V after the reacquisition of the electrons that were lost during the oxidation process at high voltage values.

The surface of the electrodes was investigated by X-ray Photoelectron Spectroscopy (XPS). This way, the XPS wide-scan for the as-prepared laminate sample only detected C, F and a little amount of O and S elements. On the contrary, Fe and Na were not observed on the surface. Consequently, it could be suspected that the $Na_{2.5}Fe_{1.75}(SO_4)_3$ active material is well coated by the carbonaceous components and PVdF. Table 1 shows the obtained atomic percentage data of all the elements (C, O, Na, F, S and P) for the initial laminate and the discharged and charged electrodes. For the charged and the discharged samples, significant quantities of C, F and O were detected. Moreover, a noticeable amount of Na was noted, as well as small amounts of S and P. High resolution C 1s, O 1s, Na 1s and F 1s XPS spectra were recorded for the three samples as shown in Fig. 7.

The C 1*s* photoemission line for the three samples presents a main peak located at 284.6 eV. This signal is assigned to the graphitic-like compounds constituting the composite, such as graphene and Ketjen Black. The signals from the PVdF binder are also clearly observed in all cases: the peak located at 290.7 eV corresponds to the -CF_2- group and the one at 286.1 eV can be ascribed to the -CH_2- group. However, the cycled electrodes show a new contribution ascribed to the C-O binding energy situated at ~285.8 eV. In addition, it is remarkable that the C 1*s* photoemission lines of the cycled electrodes show less intensity than that observed for the initial laminate.

The O 1*s* spectra are featured in Fig. 7b. In the initial state, few oxygen atoms are present on the surface of the sample. Those few atoms probably form part of some of the functional groups concerning the Ketjen Black and/or graphene species. After cycling the electrodes, the oxygen signal shifts to slightly higher binding energies. Additionally, the intensity of the band augments as a result of the increased number of O atoms on the surface. This fact clearly suggests that a Solid-Electrolyte Interphase (SEI) is formed. This SEI is probably composed of sodium carbonate (~532.8 eV) and alkyl-carbonate (~534 eV and ~532.9 eV) compounds, along with PEO (~533 eV) [24], which could be a result of the polymerization of the EC solvent [25].

The Na 1*s* photoelectron line present in the charged and discharged states (Fig. 7c), corresponds to sodium carbonate and sodium alkyl-carbonate (~ 1072.6 eV) compounds, being these results in good agreement with C 1*s* and O 1*s* spectra. Additionally, traces of NaF can also be detected for the charged sample at higher binding energies. The slight energy raise observed for the main photoemission line of Na 1s in the case of the charged electrode, would be originated by the oxidized condition of whole material at 4.5 V, which unquestionably would affect the chemical bond of the Na^+ ions on the surface of the material.

The main component of the F 1*s* XPS peak (Fig. 7d) of the initial laminate corresponds to the -CF_2- group of the PVdF (~ 687.8 eV). During the electrochemical cycling, this signal remains visible but it experiments an attenuation as a result of the SEI formation. The charged sample contains the greater amount of F on the surface and the main signal is located at ~687 eV. This signal corresponds to the PF_6^- species constituting the electrolyte, which have been deposited on the electrode surface as a consequence of graphene oxidation. For the discharged material, the amount of F is decreased but the XPS signal becomes broader due the sum of several contributions, such as PVdF, PF_6^- and traces of NaF (~ 684.5 eV).

Table 1
Atomic percentage data of all the elements obtained by XPS for the initial laminate, and the discharged and charged electrodes.

Atomic %	C	O	Na	F	S	P
Laminate	76%	5%	~0%	18%	1%	0%
Charged	33%	19%	8%	34%	2%	4%
Discharged	42%	24%	7%	21%	2%	4%

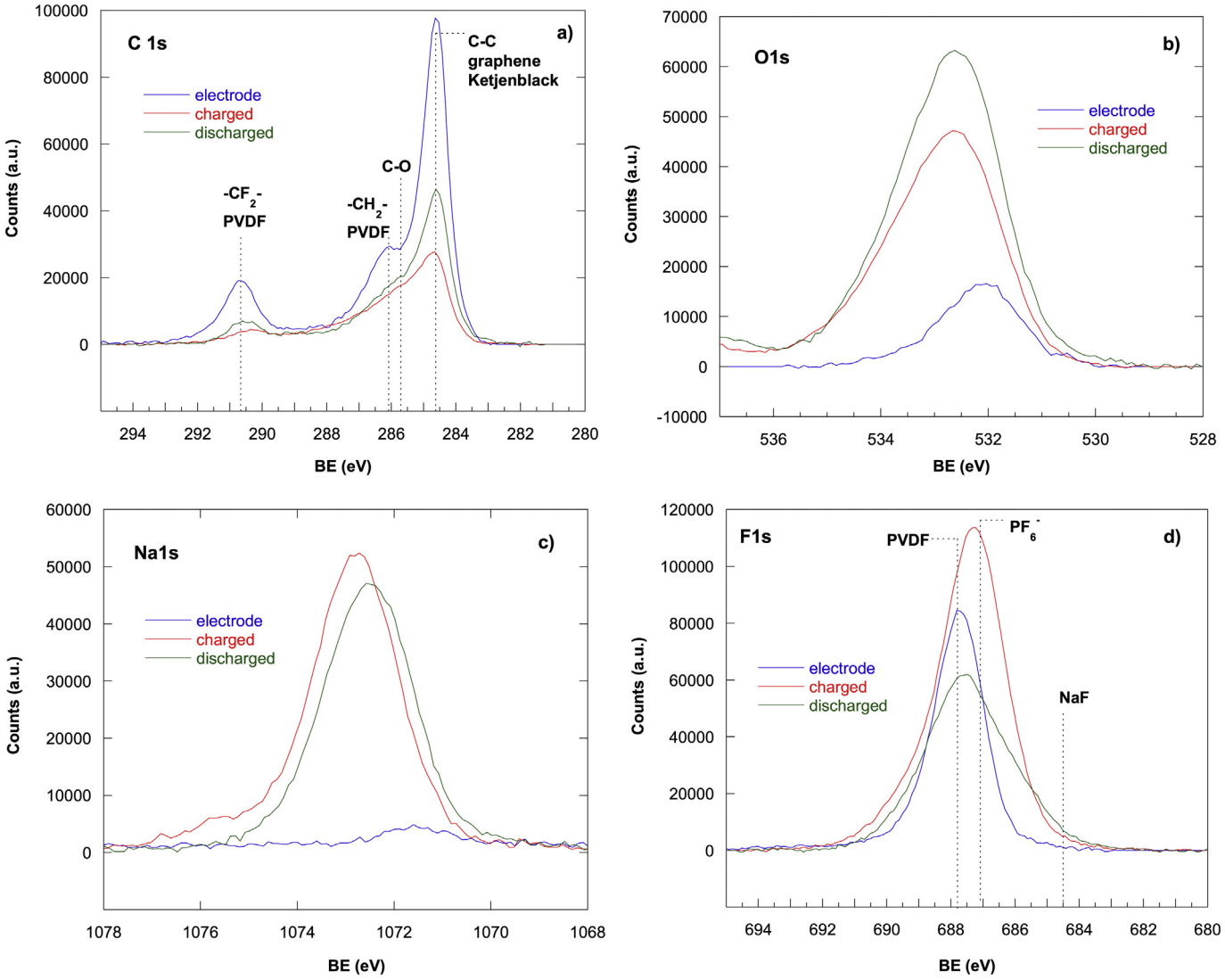

Fig. 7. High resolution XPS spectra of the as prepared laminate, and the charged and discharged electrodes: a) C 1s, b) O 1s, c) Na 1s and d) F 1s.

Taking into account the XPS results and the morphology observed by TEM micrographs for the electrode material, the schematic picture in Fig. 8 could illustrate the SEI layer formation on the $Na_{2.5}Fe_{1.75}(SO_4)_3$/Ketjen/rGO composite surface upon cycling. Before assembling the coin cells, the pristine electrode presents a carbonaceous surface mainly composed by graphene and Ketjen Black carbon constituents as well as the PVdF binder. Meanwhile, the active sulfate compound stays at a deeper layer of the composite.

On the other hand, once the electrode is cycled, the carbon coating that stands on the surface reacts with the electrolyte yielding a new cover layer composed by a mixture of sodium carbonate, sodium alkyl-carbonate and probably some PEO. At the charged state, the PF_6^- ions coming from the salt of the electrolyte are connected with the oxidized graphene in order to maintain the electroneutrality. On discharge, partial-decomposition products coming from $NaPF_6$, such as $Na_zPF_xO_y$ and NaF, start to materialize. At this point, the graphitic peak situated at 284.6 eV and the PVdF signals undergo an intensity reduction but they still remain visible after the SEI formation. This way, it could be suspected that the formed SEI layer will have a thin thickness ($\ll$ 10 nm which is the depth scope of the XPS technique) or that it might have an inhomogeneous nature. It would be advisable to obtain additional experimental results to justify the proposed SEI model. In this regard, it is remarkable that the post mortem study of the electrode samples is usually complicated due to the amorphous character of the numerous compounds that are formed throughout cycling. Considering the great stability and the good electrochemical performance provided by the composite, it can be concluded that a stable SEI layer has been formed guaranteeing the protection of the electrode and slowing down the degradation process.

4. Conclusions

An advanced cathode composite, $Na_{2.5}Fe_{1.75}(SO_4)_3$/Ketjen/rGO, has been successfully prepared for SIBs by combining the excellent electrochemical properties of the off-stoichiometric iron sulfate alluaudite, the reduced graphene oxide and the Ketjen Black carbon. As a result, a high quality electrode material constituted by a porous sulfate core properly coated by interweaved rGO fibers and Ketjen Black nanoparticles, has been obtained, as demonstrated by TEM and SEM. The post-mortem study has revealed that the carbonaceous coating generates a stable and protective SEI layer over the active material promoting a successful performance of the

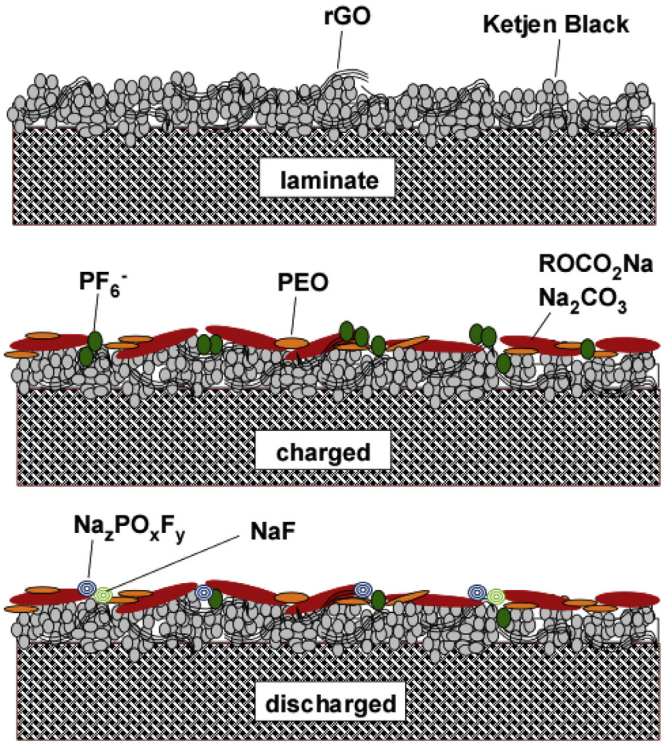

Fig. 8. Schematic picture of the electrode surface and the SEI layer formed on $Na_{2.5}Fe_{1.75}(SO_4)_3$/Ketjen/rGO composite surface upon cycling.

composite during a long cycle life. Thus, in this work the potential application of alluaudite based sulfate compounds for high voltage cathode application in SIBs has been demonstrated. Therefore, $Na_{2.5}Fe_{1.75}(SO_4)_3$/Ketjen/rGO composite is an excellent candidate in order to replace the conventional cathodes towards the development of next generation SIBs.

Acknowledgment

This work was financially supported by the Ministerio de Economía y Competitividad (MAT2016-78266-P) and Gobierno Vasco/Eusko Jaurlaritza (CICE2017). The authors thank for technical and human support provided by SGIker of UPV/EHU and European funding (ERDF and ESF). A.I. thanks the Gobierno Vasco/Eusko Jaurlaritza for a fellowship.

Appendix A. Supplementary data

Supplementary data related to this article can be found at https://doi.org/10.1016/j.jpowsour.2017.09.087.

References

[1] C.P. Grey, J.M. Tarascon, Sustainability and *in situ* monitoring in battery development, Nat. Mater. 16 (2017) 45–56.
[2] V. Palomares, M. Casas-Cabanas, E. Castillo-Martínez, M.H. Han, T. Rojo, Update on Na-based battery materials. A growing research path, Energ. Environ. Sci. 6 (2013) 2312–2337.
[3] V. Palomares, P. Serras, I. Villaluenga, K.B. Hueso, J. Carretero-González, T. Rojo, Na-ion batteries, recent advances and present challenges to become low cost energy storage systems, Energ. Environ. Sci. 5 (2012) 5884–5901.
[4] M.H. Han, E. Gonzalo, G. Singh, T. Rojo, A comprehensive review of sodium layered oxides: powerful cathodes for Na-ion batteries, Energ. Environ. Sci. 8 (2015) 81–102.
[5] J.-Y. Hwang, S.-T. Myung, Y.-K. Sun, Sodium-ion batteries: present and future, Chem. Soc. Rev. 46 (2017) 3529–3614.
[6] J. Lu, S.-I. Nishimura, A. Yamada, Polyanionic solid-solution cathodes for rechargeable batteries, Chem. Mater. 29 (2017) 3597–3602.
[7] P. Barpanda, G. Oyama, S.-I. Nishimura, S.C. Chung, A. Yamada, A 3.8-V earth-abundant sodium battery electrode, Nat. Commun. (2014), https://doi.org/10.1038/ncomms5358.
[8] O. Oyama, S.-I. Nishimura, Y. Suzuki, M. Okubo, A. Yamada, Off-stoichiometry in alluaudite-type sodium iron sulfate $Na_{2+2x}Fe_{2-x}(SO_4)_3$ as an advanced sodium battery cathode material, ChemElectroChem 2 (2015) 1019–1023.
[9] S.-I. Nishimura, Y. Suzuki, J. Lu, S. Torii, T. Kamiyama, A. Yamada, High-temperature neutron and X-ray diffraction study of fast sodium transport in alluaudite-type sodium iron sulfate, Chem. Mater. 28 (7) (2016) 2393–2399.
[10] G. Oyama, H. Kiuchi, S.C. Chung, Y. Harada, A. Yamada, Combined experimental and computational analyses on the electronic structure of alluaudite-type sodium iron sulfate, J. Phys. Chem. C 120 (2016) 23323–23328.
[11] L.L. Wong, H.M. Chen, S. Adams, Sodium-ion diffusion mechanisms in the low cost high voltage cathode material $Na_{2+\delta}Fe_{2-\delta/2}(SO_4)_3$, Phys. Chem. Chem. Phys. 17 (2015) 9186–9193.
[12] G. Oyama, O. Pecher, K.J. Griffith, S. Nishimura, R. Pigliapochi, C.P. Grey, A. Yamada, Sodium intercalation mechanism of 3.8 V class alluaudite sodium iron sulfate, Chem. Mater. 28 (2016) 5321–5328.
[13] D. Dwibedi, C.D. Ling, R.B. Araujo, S. Chakraborti, S. Duraisamy, N. Munichandraiah, R. Ahuja, P. Barpanda, Ionothermal synthesis of high-voltage alluaudite $Na_{2+2x}Fe_{2-x}(SO_4)_3$ sodium insertion compound: structural, electronic, and magnetic insights, ACS Appl. Mater. Interfaces 8 (2016) 6982–6991.
[14] Y. Meng, T. Yu, S. Zhang, C. Deng, Top-down synthesis of muscle-inspired alluaudite $Na_{2+2x}Fe_{2-x}(SO_4)_3$/SWNT spindle as a high-rate and high-potential cathode for sodium-ion batteries, J. Mater. Chem. A 4 (2016) 1624–1631.
[15] T. Yu, B. Lin, Q. Li, X. Wang, W. Qu, S. Zhang, C. Deng, First exploration of freestanding and flexible $Na_{2+2x}Fe_{2-x}(SO_4)_3$@porous carbon nanofiber hybrid films with superior sodium intercalation for sodium ion batteries, Phys. Chem. Chem. Phys. 18 (2016) 26933–26941.
[16] K.S. Novoselov, V.I. Fal'ko, L. Colombo, P.L. Gellert, M.G. Schwab, K. Kim, A roadmap for graphene, Nature 490 (2012) 192–200.
[17] D. Yan, X. Xu, T. Lu, B. Hu, D.H.C. Chua, L. Pan, Reduced graphene oxide/carbon nanotubes sponge: a new high capacity and long life anode material for sodium-ion batteries, J. Power Sources 316 (2016) 132–138.
[18] J. Rodríguez-Carvajal, Fullprof program, Phys. B 192 (1993) 55. http://www.ill.eu/sites/fullprof/.
[19] N.A. Kumar, R.R. Gaddam, S.R. Varanasi, D. Yang, B.X.S. Zhao, Sodium ion storage in reduced graphene oxide, Electrochim. Acta 214 (2016) 319–325.
[20] D. Dwibedi, R.B. Araujo, S. Chakraborty, P.P. Shanbogh, N.G. Sundaram, R. Ahuja, P. Barpanda, $Na_{2.44}Mn_{1.79}(SO_4)_3$: a new member of the alluaudite family of insertion compounds for sodium ion batteries, J. Mater. Chem. 3 (2015) 18564–18571.
[21] P. Cui, J. Lee, E. Hwang, H. Lee, One-pot reduction of graphene oxide at subzero temperatures, Chem. Commun. 47 (2011) 12370–12372.
[22] K. Nakamoto, Infrared and Raman Spectra of Inorganic and Coordination Compounds: Part A: Theory and Applications in Inorganic Chemistry, sixth ed., Wiley, 2008.
[23] T. Placke, G. Schmuelling, R. Kloepsch, P. Meister, O. Fromm, P. Hilbig, H.-W. Meyer, M. Winter, In situ X-ray diffraction studies of cation and anion intercalation into graphitic carbons for electrochemical energy storage applications, Z. Anorg. Allg. Chem. 640 (10) (2014) 1996–2006.
[24] L. Ji, M. Gu, Y. Shao, X. Li, M.H. Engelhard, B.W. Arey, W. Wang, Z. Nie, J. Xiao, C. Wang, J.-G. Zhang, J. Liu, Controlling SEI formation on SnSb-porous carbon nanofibers for improved Na ion storage, Adv. Mater 26 (2014) 2901–2908.
[25] M.A. Muñoz-Marquez, M. Zarrabeitia, E. Castillo-Martínez, A. Eguía-Barrio, T. Rojo, M. Casas-Cabanas, Composition and evolution of the solid-electrolyte interphase in $Na_2Ti_3O_7$ electrodes for Na-Ion batteries: XPS and auger parameter analysis, ACS Appl. Mater. Interfaces 7 (2015) 7801–7808.